Computational and Experimental Fatigue Analysis of Contoured Spinal Rods

Agnese Piovesan[1]
Laboratory of Biological Structure Mechanics,
Department of Chemistry, Materials and
Chemical Engineering "Giulio Natta",
Politecnico di Milano,
Piazza Leonardo da Vinci 32,
Milan 20133, Italy

Francesca Berti[1]
Laboratory of Biological Structure Mechanics,
Department of Chemistry, Materials and
Chemical Engineering "Giulio Natta",
Politecnico di Milano,
Piazza Leonardo da Vinci 32,
Milan 20133, Italy

Tomaso Villa
Laboratory of Biological Structure Mechanics,
Department of Chemistry, Materials and
Chemical Engineering "Giulio Natta",
Politecnico di Milano,
Piazza Leonardo da Vinci 32,
Milan 20133, Italy

Giancarlo Pennati
Laboratory of Biological Structure Mechanics,
Department of Chemistry, Materials and
Chemical Engineering "Giulio Natta",
Politecnico di Milano,
Piazza Leonardo da Vinci 32,
Milan 20133, Italy

Luigi La Barbera[2]
Laboratory of Biological Structure Mechanics,
Department of Chemistry, Materials and
Chemical Engineering "Giulio Natta",
Politecnico di Milano,
Piazza Leonardo da Vinci 32,
Milan 20133, Italy
e-mail: luigi.labarbera@polimi.it

Posterior fixation with contoured rods is an established methodology for the treatment of spinal deformities. Both uniform industrial preforming and intraoperative contouring introduce tensile and compressive plastic deformations, respectively, at the concave and at the convex sides of the rod. The purpose of this study is to develop a validated numerical framework capable of predicting how the fatigue behavior of contoured spinal rods is affected by residual stresses when loaded in lordotic and kyphotic configurations. Established finite element models (FEM) describing static contouring were implemented as a preliminary simulation step and were followed by subsequent cyclical loading steps. The equivalent Sines stress distribution predicted in each configuration was compared to that in straight rods (SR) and related to the corresponding experimental number of cycles to failure. In the straight configuration, the maximum equivalent stress (441 MPa) exceeds the limit curve, as confirmed by experimental rod breakage after around 1.9×10^5 loading cycles. The stresses further increased in the lordotic configuration, where failure was reached within 2.4×10^4 cycles. The maximum equivalent stress was below the limit curve for the kyphotic configuration (640 MPa), for which a run-out of 10^6 cycles was reached. Microscopy inspection confirmed agreement between numerical predictions and experimental fatigue crack location. The contouring technique (uniform contouring (UC) or French bender (FB)) was not related to any statistically significant difference. Our study demonstrates the key role of residual stresses in altering the mean stress component, superposing to the tensile cyclic load, potentially explaining the higher failure rate of lordotic rods compared to kyphotic ones.
[DOI: 10.1115/1.4042767]

Keywords: spinal rods, contouring, residual stresses, fatigue, Ti6Al4V

1 Introduction

Posterior fixation is a well-established technique in spinal surgery, particularly for deformities and instability correction [1–6]. Rods are widely used to restore physiological spine curvature and maintain a well-balanced condition. Although preformed spinal rods, obtained through industrial contouring, are currently available in the market [2], intraoperative contouring is generally performed by surgeons before implantation to achieve satisfactory matching with a patient's spinal curvature. Tools capable of inducing permanent plastic deformation or residual stress, i.e., French benders (FB) [7], are typically used.

Although simple analytic calculations based on a well-established elastoplastic beam theory would allow one to evaluate the stresses arising during contouring, this approach is limited both to static loading and to rather simple planar bending conditions. A recent study [8] established a numerical workflow capable of describing the residual stress distributions arising in a spinal rod following both the clinical contouring with a French bender and the industrial preforming. The latter was achieved using a four-point bending bench capable of inducing uniform curvature and homogeneous contouring over the wide portion of the rod demarcated by the loading pins. As expected, spinal rod contouring induced residual tensile stresses along the concave side while compression was found along the convex one [8]; however, the study interestingly quantified the complex triaxial stress state produced under the loading pin with a French bender, hardly evaluable with an analytical approach. Many efforts have been made to experimentally study the effects of static contouring and material properties both on static [9,10] and on fatigue performances [11–13], but a clear correlation between the residual stress distributions of a contoured spinal rod and its fatigue behavior has not been determined yet.

In the literature, a high rod breakage rate due to mechanical fatigue has been reported [1–3,5,6,14], with the lumbar region being significantly more susceptible than the thoracic one [14]. The relatively higher lumbar loads (e.g., body weights, muscle forces) [15,16] only partially explain these results. Nonetheless, recent studies [4,17,18] demonstrated that the loads experienced by rods subjected to physiological loading conditions during every-day life are much lower than the material strength, and are not sufficient to justify the observed fatigue failure rate. Therefore, we may infer that the initial residual stress distribution induced by contouring, combined with the bending loading direction (lordotic or kyphotic), could better explain the observed clinical failures.

The purpose of this study is thus to develop a validated numerical framework capable of predicting how the fatigue behavior of

[1]Agnese Piovesan and Francesca Berti contributed equally.
[2]Corresponding author.
Manuscript received October 5, 2018; final manuscript received January 29, 2019; published online February 25, 2019. Assoc. Editor: Anton E. Bowden.

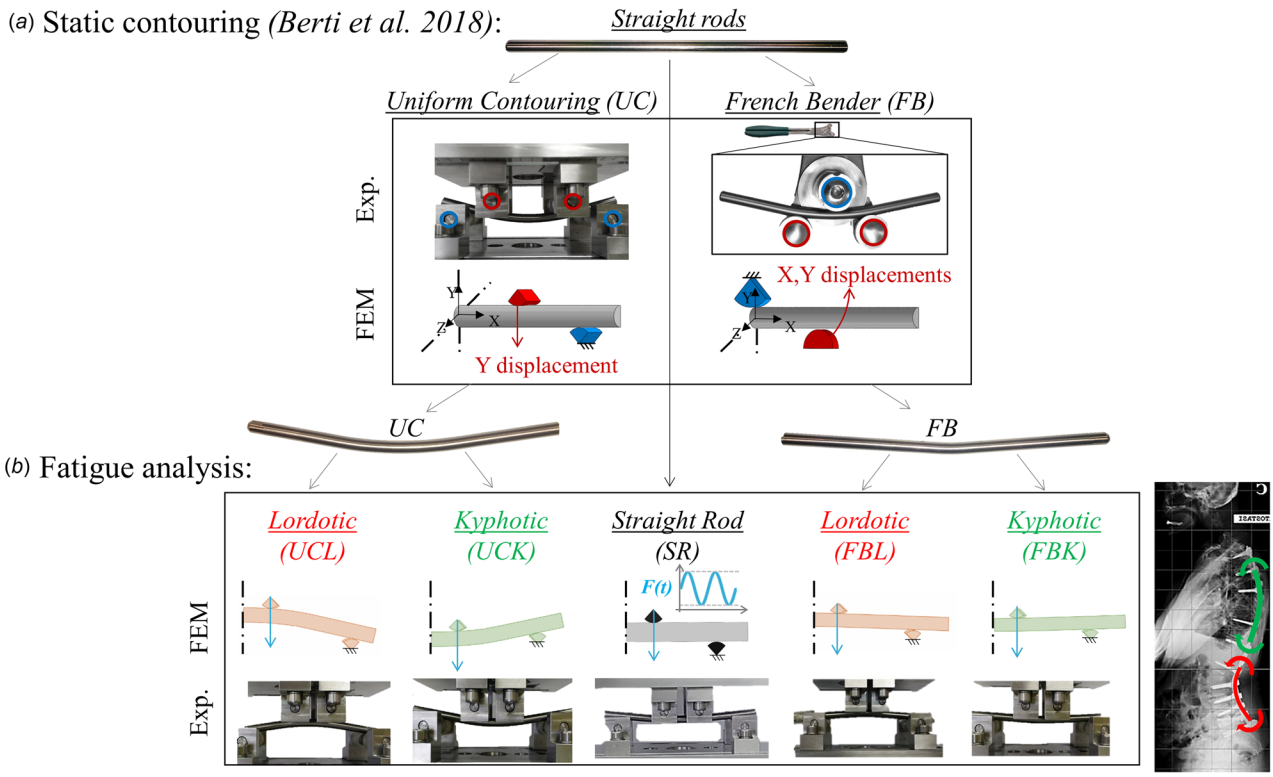

Fig. 1 Work flow of computational (FEM) and experimental (Exp.) analysis: preliminary static contouring steps (*a*) based on French bender (FB) and uniform four-point bending contouring (UC) [8]; (*b*) subsequent fatigue steps for straight and contoured spinal rods according to lordotic and kyphotic configurations

contoured spinal rods will be affected by residual stresses. Special attention is paid to the role played by residual stresses when the rod is loaded according to a kyphotic or lordotic configuration, where the tensile and compressive residual stresses are on opposite sides. Established finite element models (FEM) [8] simulating both FB and uniform contouring (UC) are employed as preliminary steps. Contoured models are subjected to subsequent cyclical loading steps; then numerical results are compared to results of dynamic experimental tests.

2 Materials and Methods

Spinal rod fatigue behavior following contouring was investigated through both FE models and experimental tests; Ti6Al4V ELI-grade spinal rods with 5.5 mm diameter (Leghe Leggere Lavorate s.r.l., Milan, Italy) were used. The samples employed in all experimental tests of the study consisted of 100 mm length rod segments.

2.1 Computational Fatigue Performance Evaluation. To better understand the role of the residual stresses introduced by static contouring on fatigue performance (Fig. 1(*a*)), the rods were loaded in a four-point-testing setup representing a kyphotic and a lordotic configuration. This loading resulted in either concave or convex rods, respectively, to which cyclic bending was applied (Fig. 1(*b*)).

Five different configurations were compared:

- straight rod, reference condition;
- uniformly contoured rod loaded in kyphotic configuration (UCK);
- uniformly contoured rod loaded in lordotic configuration (UCL);
- rods contoured through French bender loaded in kyphotic configuration (FBK); and
- rods contoured through French bender loaded in lordotic configuration (FBL).

Structural FE models were built to describe each testing conditions. The meshing strategy, material properties, and contact properties for both the spinal rod and the loading/support pins were implemented as previously reported [8]; only the position of the loading pins was adjusted to match the experimental setup. A release step was added after the preliminary static contouring step [8]. To preserve information about the residual stresses and strains, three loading cycles were implemented as subsequent steps, alternating loading (peak) and unloading (valley). A triangular displacement was assigned to the loading pins, resulting in a reaction force within 1% of the experimental force values.

The peak and valley stress tensors were extracted on the last cycle for all the nodes within the gauge length. Data were exported to MATLAB R2016b (MathWorks, Natick, MA). An ad hoc script was implemented to study the risk of fatigue failure for each configuration. The fatigue analysis—in terms of failed/not failed—was achieved by constructing the constant life diagram at 10^6 cycles (Haigh diagram).

The stress components were combined according to the Sines' criterion, recommended for Titanium alloys and metals in general [19]

$$\sigma_{\text{SINES}} = \sigma_{\text{VM},a} + K \times I_m \tag{1}$$

where the alternate component of the von Mises stress ($\sigma_{\text{VM},a}$) and the average component of the hydrostatic stress (I_m) were calculated as follow:

$$\sigma_{\text{VM},a} = \sqrt{\frac{1}{2}\left[(\sigma_{1,a} - \sigma_{2,a})^2 + (\sigma_{1,a} - \sigma_{3,a})^2 + (\sigma_{2,a} - \sigma_{3,a})^2\right]} \tag{2}$$

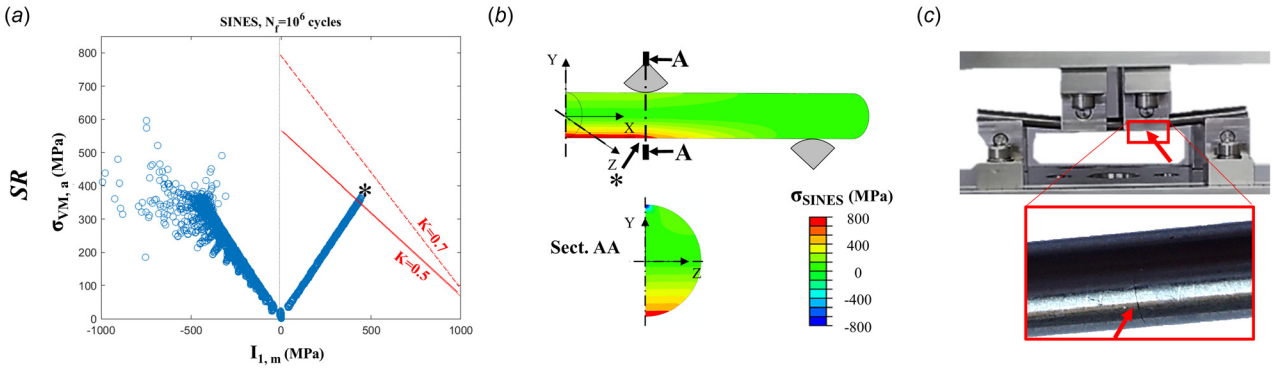

Fig. 2 (*a*) **Constant life diagram at 1×10^6 cycles for the SR: limit curves are shown for $K = 0.5$ (solid line) and $K = 0.7$ (dashed line);** (*b*) **equivalent Sines stress map, with maximum value pointed out by an arrow; and** (*c*) **experimental failure mechanism**

Table 1 Stress components predicted at each simulated step at the most loaded location and the experimental numbers of cycles to failure are compared in each configuration. For the fatigue analysis, the average component of the first invariant of the stresses (I_m), the von Mises alternated stress ($\sigma_{VM,a}$), and the resulting Sines equivalent stress (σ_{SINES}) are reported.

	Fatigue analyses										
	Stress components (MPa)						Max Sines stress (MPa)			Fatigue experiments	
	Peak		Valley		Cycles		σ_{SINES} (K)			Number of cycles to failure (cycles)	
Configuration	P	σ_{VM}	P	σ_{VM}	I_m	$\sigma_{VM,a}$	$K = 0.5$	$K = 0.55$	$K = 0.7$	Median	Std. Dev.
SR	266	818	28	86	441	366	587	609	675	196,118	548,148
UCL	380	1111	130	384	765	363	746	784	899	24,236	15,766
UCK	−308	1085	161	71	−201	507	407	396	366	0	0
FBL	352	944	100	216	678	364	703	737	839	24,495	5421
FBK	202	577	−34	91	253	334	461	473	512	0	0

$$I_m = \sigma_{1,m} + \sigma_{2,m} + \sigma_{3,m} = 3P_m \tag{3}$$

where $\sigma_{1,m}, \sigma_{2,m}, \sigma_{3,m}$ are the mean principal stresses, $\sigma_{1,a}, \sigma_{2,a}, \sigma_{3,a}$ are the alternate principal stresses—namely the eigenvalues of the mean and alternate stress tensors respectively—and P_m is the hydrostatic pressure. Mean and alternate stresses tensors were computed from the principal stress tensors at fatigue peak and valley as

$$\sigma_{ij,m} = \frac{\left(\sigma_{ij}^{\text{peak}} + \sigma_{ij}^{\text{valley}}\right)}{2} \tag{4}$$

$$\sigma_{ij,a} = \frac{\left(\sigma_{ij}^{\text{peak}} - \sigma_{ij}^{\text{valley}}\right)}{2} \tag{5}$$

In Eq. (1), the K parameter can assume a range of values dependent on the material grain size and surface roughness; K is defined by the ratio $(\sigma_{FA,f}/\sigma_R)$, where σ_R is the material ultimate strength as obtained in tensile tests [8], while $\sigma_{FA,f}$ indicates the maximum alternating load resulting in infinite fatigue life for $R = -1$. For Ti6Al4V, a reasonable value could be set between 0.5 and 0.7 [20,21], and the distribution of Sines equivalent stress will be displayed assuming $K = 0.5$.

2.2 Experimental Fatigue Tests. Excluding other implant components, the contoured rods were experimentally tested under cyclic loading conditions using a highly reproducible four-point bending setup. The distance between the loading pins was set to 20 mm to avoid the stress intensification effects resulting from loading-pin indentation induced during the previous static step on UC rods [8]. Such a configuration allowed application of a constant bending moment in the middle portion of the sample (gauge length) always including the contoured region of both FB and UC rods.

Five specimens were tested for each configuration, setting a run-out of 10^6 (roughly one year of use). Fatigue tests were carried out at 10 Hz through the MTS testing machine (858 MiniBionix, MTS System Inc., Minneapolis, MN). Load control was used and a sinusoidal shape up to 930 N was applied with a load ratio $R = 0.1$. The load was set to ensure failure of the straight rods in a reasonable time. The tests were performed until fracture or run-out. Specimens were inspected with optical microscopy (Nikon SMZ800 stereo microscope, Nikon Corporation, Tokyo, Japan) after testing. The results were expressed in terms of fatigue life (number of cycles to failure) and failure location. A nonparametric Mann–Whitney test was used to assess any statistical difference between fatigue life of both the lordotic and kyphotic rods contoured using the FB and UC methods ($p = 0.05$).

3 Results

3.1 Computational Fatigue Performance Evaluation. Because most of the points in the gage length of the SR experienced a constant load ratio during dynamic loading, the constant life (Haigh) diagram was perfectly straight in traction; points were more dispersed in compression, due to the expected multiaxial stress state affecting the elements under the loading pin. Some elements belonging to the gage length fell beyond the limit curve on the Haigh diagram, thus suggestive of rod fatigue failure for $K \leq 0.55$ (Fig. 2(*a*)). The element experiencing the maximum Sines stress of 609 MPa (Table 1) corresponded to the opposed side of the loading pin location undergoing traction (Fig. 2(*b*)). The experimental fractures confirmed the localization predicted numerically (Fig. 2(*c*)).

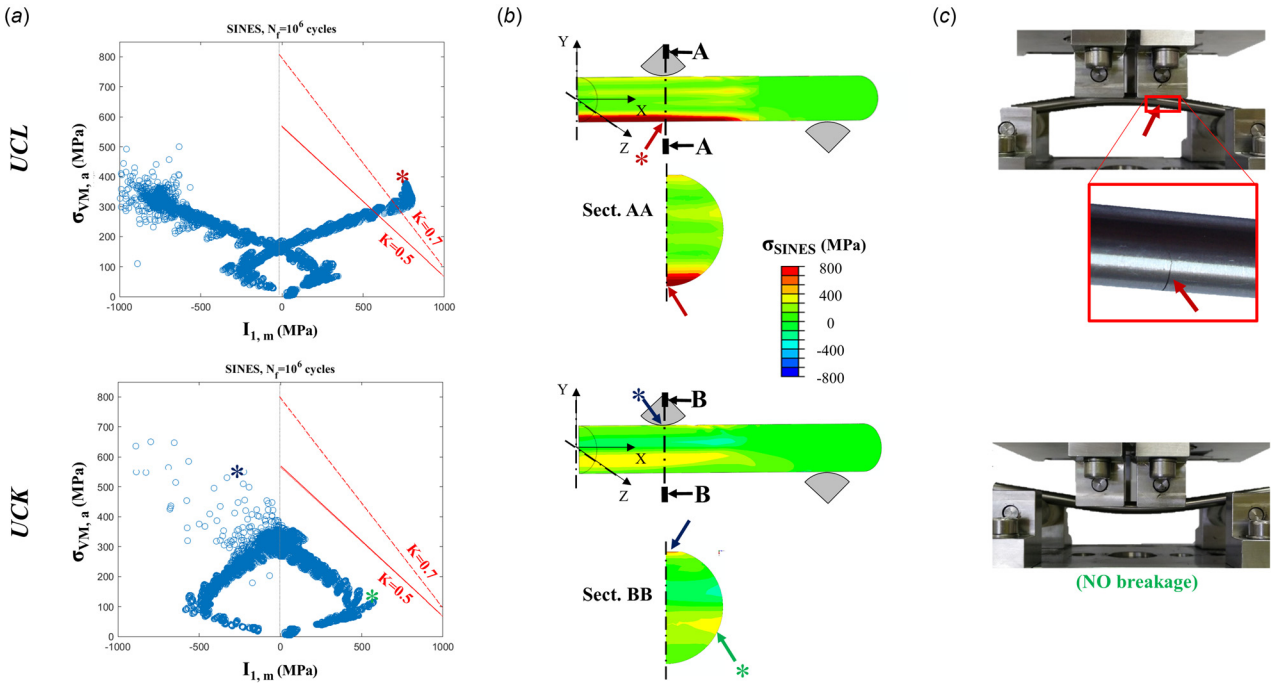

Fig. 3 (*a*) Constant life diagrams at 1×10^6 cycles for the uniform contouring specimens, in both the lordotic (UCL) and kyphotic (UCK) configurations: limit curves are shown for $K = 0.5$ (solid line) and $K = 0.7$ (dashed line); (*b*) equivalent Sines stress maps, with maximum value pointed out by an arrow; and (*c*) experimental failure mechanism, if any

The Haigh diagram was more dispersed in UC and FB configurations because different halves of the cross section initially experienced tensile/compressive residual stresses at the concave/convex regions; moreover, the load ratio upon loading varied from element to element due to loading pin indentation. The lordotic configurations demonstrated stress components exceeding the limit curves of the Haigh diagram (Fig. 3(*a*), top). UCL configuration demonstrated a 27% increase in maximum Sines stress compared to the reference condition, with a 73% increase in the mean stress component, while the alternate component was almost unvaried (Table 1). The maximum Sines stress value was found in the same location as for the SR, but here the dynamic load contributes to increasing tension at the concave side, being superposed on the tensile residual stresses induced by static contouring (Fig. 3(*b*), top). During the fatigue test, the fractures occurred at the same location predicted by the model (Fig. 3(*c*)). In FBL configuration, the maximum Sines stress value increased by 20% compared to the reference configuration, mainly due to the mean stress component rising by 54% (Table 1). The highest loaded region was successfully predicted slightly peripheral to the French bender notch were the static contouring induces tensile residual stresses (Figs. 4(*b*) and 4(*c*), top).

On the contrary, the spinal rods loaded in kyphotic configuration showed no points exceeding the limit curve (Figs. 3(*a*) and 4(*a*), bottom), because the dynamic load contributes to increasing tension at the convex side, superposed on the compressive residual stresses induced by static contouring. In UCK configuration, the maximum Sines equivalent stress decreased by 31% compared to the straight configuration, even though the alternate component increases by 38%, because the mean component achieves negative values (Table 1). A 21% decrease in the maximum Sines stress was predicted for FBK, resulting from a combination of decreases in both alternate and mean components by 9% and 43%, respectively.

3.2 Experimental Fatigue Tests. Both kyphotic configurations reached the run-out, demonstrating greater fatigue strength than both straight and lordotic rods configurations (Table 1). Lordotic configurations were found to be the most susceptible to fatigue failure, with a significantly lower number of cycle to failure than the reference configuration ($p = 0.012$ in both cases); on the other hand, no statistical difference was found between UCL and FBL ($p > 0.05$). Despite reaching the run-out without any functional failure, all UCK samples demonstrated some microcracks on the compression side of the rod, just below the loading pins.

4 Discussion

The current study investigated the role of residual stresses induced by alternative contouring techniques on the fatigue resistance of contoured spinal rods. The combined numerical-experimental approach already established in a previous study to describe static contouring [8] was here assumed as a preliminary step, and then extended to include subsequent cyclical loading steps.

All the results from the numerical contouring models agreed with the experimental tests, both in terms of fatigue failure assessments and crack location, in addition to K value; in particular, for straight rods, the K value predicting failure was 0.55, which is within the reported literature data for typical Ti6Al4V [20,21]. The analyses proved how the lordotic configuration was the most susceptible to failure while the kyphotic one appeared safest. This numerical outcome was confirmed by the observation that lordotic rods failed experimentally while kyphotic ones reached the predefined run-out. No statistical difference was found between the number of cycles to failure for spinal rods contoured using alternative techniques (UC or FB): the maximum Sines stress reached in the two configurations was comparable, with maximum differences of 6%. Although a previous study highlighted specific differences between these techniques [8], the current analysis confirmed the importance of the amount of rod contouring (i.e., curvature radius) rather than the bending technique itself.

Although other authors have focused mainly on the severity of rod contour [11–13] and on notch effect [22,23] induced by French bender and in situ contouring, our results support the idea that residual stresses have a direct implication in increasing or decreasing fatigue resistance. The main influence of the French bender notch resulted in slight shift of the crack initiation region

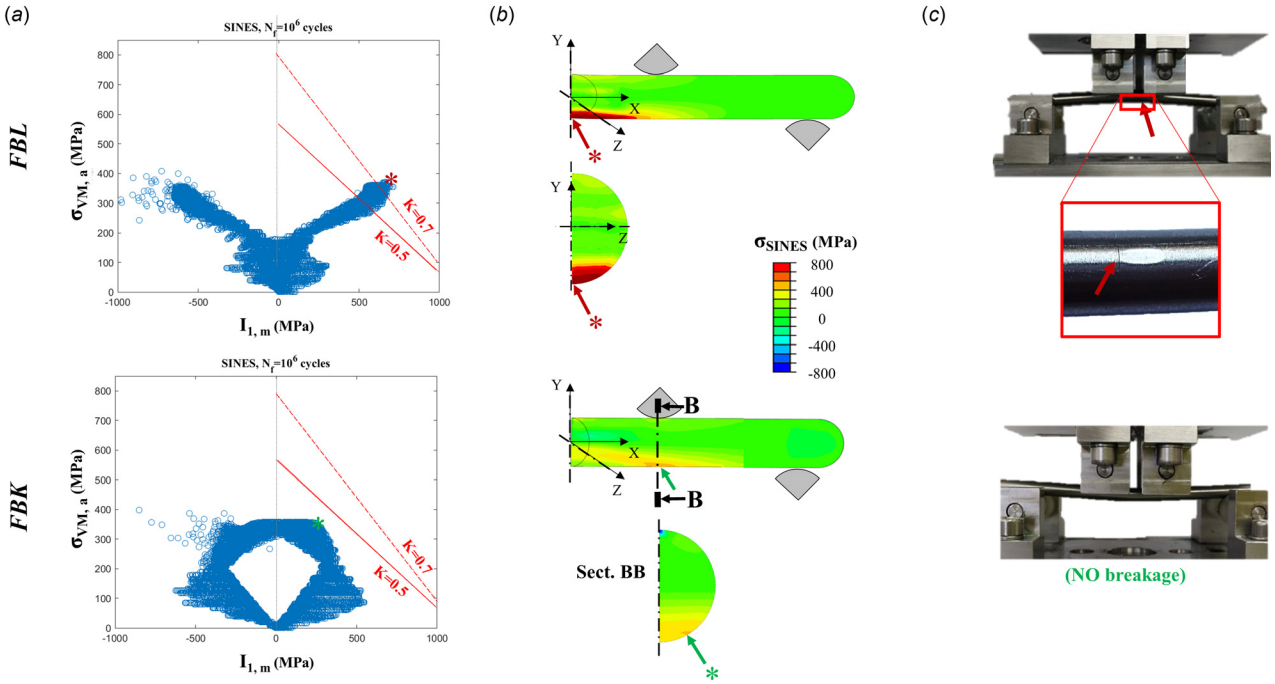

Fig. 4 (*a*) **Constant life diagrams at 1×10^6 cycles for the French bender specimens, in both the lordotic and kyphotic configurations: limit curves are shown for $K = 0.5$ (solid line) and $K = 0.7$ (dashed line); (*b*) equivalent Sines stress maps, with maximum value pointed out by an arrow; and (*c*) experimental failure mechanism, if any**

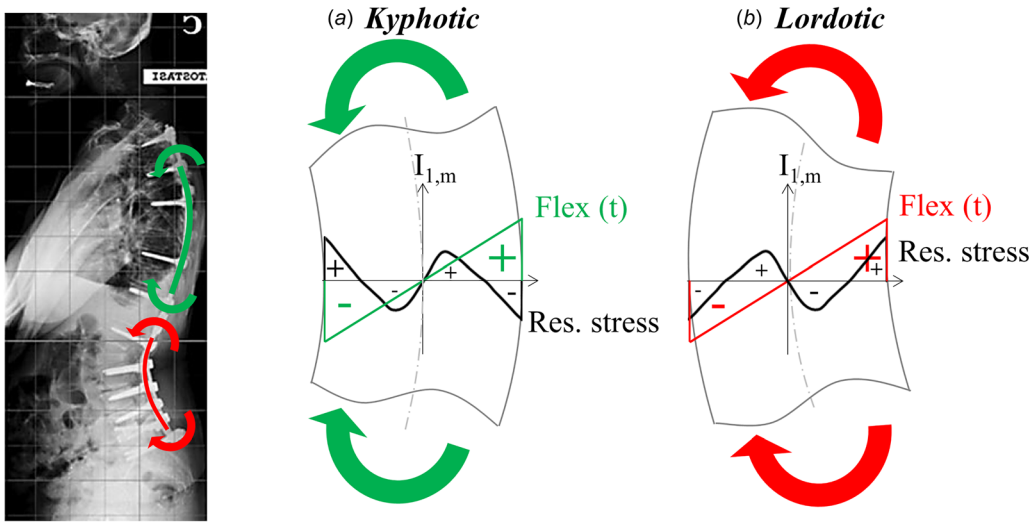

Fig. 5 Qualitative representation of the mean residual stress due to static contouring with tension/compression at the concave/convex sides and superposition of a time-dependent dynamic stress component due to flexion: these contributions sum in lordotic configuration, overcoming the fatigue limit, while they balance in kyphotic condition

in the periphery of the notched spot, where the principal stresses were tensile and the equivalent Sines stress reached the maximum value (Fig. 4).

The presence of residual stresses caused a significant alteration of the mean stress components during fatigue loading when compared to the reference configuration, where no residual stress field was present. Lordotic configurations (UCL and FBL) experienced tensile residual stresses, due to the contouring process, along their concave side, the same region undergoing cyclic tensile loads during fatigue testing (Fig. 5(*b*)). On the other hand, rods loaded in kyphotic configuration presented a compressive residual stress field at the convex side, partially compensating the tensile load arising during fatigue testing; in this light, the residual stress field produced during contouring played a role in significantly reducing the event of failure (Fig. 5(*a*)).

This study provides the mechanical rationale to demonstrate how contoured spinal rods implanted in the lordotic region are more prone to failure than the kyphotic ones [5,14], when compared at the same load level, due to the important contribution of residual stresses. Contouring-induced residual stresses expose lordotic rods to higher stresses, a condition which could be worsened by the larger amount of body weight carried at lumbar level [15,16]. Although the simple loading condition here described cannot reproduce any relevant in vivo scenario, it allowed a very

easy control of the boundary conditions, isolating the mechanical behavior of the sole spinal rod.

Although only titanium alloy was analyzed here, the current approach could be extended to other elasto-plastic materials (both metals and polymers), and furthermore applied to optimize the fatigue behavior of spinal rods undergoing contouring. Here, for the sake of simplicity, only uniform cyclic bending was considered, with contouring and cyclic loading insisting on the same plane. Future efforts could be directed at implementing the same approach for the optimization of complex patient-specific surgeries: multiple rod contouring procedures and more realistic multi-axial loading conditions should be accounted for.

5 Conclusions

This paper investigated the role of residual stresses induced by contouring on spinal rod fatigue resistance. A validated numerical approach was used to explain the contribution of residual stresses in increasing (or decreasing) the failure risk of contoured spinal rods loaded in lordotic (or kyphotic) configuration compared to a perfectly straight rod. The contouring technique itself seems to play a secondary role in determining the fatigue resistance.

Acknowledgment

The authors gratefully acknowledge the contribution of Dario Allegretti and Claudia Ottardi for their support and helpful discussions, while Max Olender (Massachusetts Institute of Technology, MA) for his help in revising the manuscript. The authors acknowledge Carlo Miglietta (2B1, s.r.l., Milan, Italy) and Davide Pizzamiglio (Leghe Leggere Lavorate, s.r.l., Milan, Italy) for providing the French bender and the spinal rods used in the experimental testing.

References

[1] Barton, C., Noshchenko, A., Patel, V., Cain, C., Kleck, C., and Burger, E., 2015, "Risk Factors for Rod Fracture After Posterior Correction of Adult Spinal Deformity With Osteotomy: A Retrospective Case-Series," Scoliosis, **10**, p. 30.

[2] Berjano, P., Bassani, R., Casero, G., Sinigaglia, A., Cecchinato, R., and Lamartina, C., 2013, "Failures and Revisions in Surgery for Sagittal Imbalance: Analysis of Factors Influencing Failure," Eur. Spine J., **22**(S6), pp. 853–858.

[3] Charosky, S., Guigui, P., Blamoutier, A., Roussouly, P., and Chopin, D., 2012, "Complications and Risk Factors of Primary Adult Scoliosis Surgery: A Multicenter Study of 306 Patients," Spine, **37**(8), pp. 693–700.

[4] Luca, A., Ottardi, C., Sasso, M., Prosdocimo, L., La Barbera, L., Brayda-Bruno, M., Galbusera, F., and Villa, T., 2017, "Instrumentation Failure Following Pedicle Subtraction Osteotomy: The Role of Rod Material, Diameter, and Multi-Rod Constructs," Eur Spine J., **26**(3), pp. 764–770.

[5] Smith, J. S., Shaffrey, E., Klineberg, E., Shaffrey, C. I., Lafage, V., Schwab, F. J., Protopsaltis, T., Scheer, J. K., Mundis, G. J., Fu, K.-M. G., Gupta, M. C., Hostin, R., Deviren, V., Kebaish, K., Hart, R., Burton, D. C., Line, B., Bess, S., Ames, C. P., and Group, I. S. S., 2014, "Prospective Multicenter Assessment of Risk Factors for Rod Fracture Following Surgery for Adult Spinal Deformity," J. Neurosurg. Spine, **21**(6), pp. 994–1003.

[6] Yang, J. S., Sponseller, P. D., Thompson, G. H., Akbarnia, B. A., Emans, J. B., Yazici, M., Skaggs, D. L., Shah, S. A., Salari, P., and Poe-Kochert, C., 2011, "Growing Rod Fractures: Risk Factors and Opportunities for Prevention," Spine, **36**(20), pp. 1639–1644.

[7] Cook, E. J., 1982, "Rod Bender," U. S. Patent No. 4474046A.

[8] Berti, F., La Barbera, L., Piovesan, A., Allegretti, D., Ottardi, C., Villa, T., and Pennati, G., 2018, "Residual Stresses in Titanium Spinal Rods: Effects of Two Contouring Methods and Material Plastic Properties," ASME J. Biomech. Eng., **140**(11), p. 111001.

[9] Demura, S., Murakami, H., Hayashi, H., Kato, S., Yoshioka, K., Yokogawa, N., Ishii, T., Igarashi, T., Fang, X., and Tsuchiya, H., 2015, "Influence of Rod Contouring on Rod Strength and Stiffness in Spine Surgery," Orthopedics, **38**(6), pp. e520–e523.

[10] Noshchenko, A., Xianfeng, Y., Armour, G. A., Baldini, T., Patel, V. V., Ayers, R., and Burger, E., 2011, "Evaluation of Spinal Instrumentation Rod Bending Characteristics for In-Situ Contouring," J. Biomed. Mater. Res. Part B, **98**(1), pp. 192–200.

[11] Tang, J. A., Leasure, J. M., Smith, J. S., Buckley, J. M., Kondrashov, D., and Ames, C. P., 2013, "Effect of Severity of Rod Contour on Posterior Rod Failure in the Setting of Lumbar Pedicle Subtraction Osteotomy (PSO): A Biomechanical Study," Neurosurgery, **72**(2), pp. 276–282.

[12] Slivka, M. A., Fan, Y. K., and Eck, J. C., 2013, "The Effect of Contouring on Fatigue Strength of Spinal Rods: Is It Okay to Re-Bend and Which Materials Are Best?," Spine Deform., **1**(6), pp. 395–400.

[13] Lindsey, C., Deviren, V., Xu, Z., Yeh, R.-F., and Puttlitz, C. M., 2006, "The Effects of Rod Contouring on Spinal Construct Fatigue Strength," Spine, **31**(15), pp. 1680–1687.

[14] Smith, J. S., Shaffrey, C. I., Ames, C. P., Demakakos, J., Fu, K. M. G., Keshavarzi, S., Carol, C. M., Deviren, V., Schwab, F. J., Lafage, V., and Bess, S., 2012, "Assessment of Symptomatic Rod Fracture After Posterior Instrumented Fusion for Adult Spinal Deformity," Neurosurgery, **71**(4), pp. 862–867.

[15] Han, K. S., Rohlmann, A., Zander, T., and Taylor, W. R., 2013, "Lumbar Spinal Loads Vary With Body Height and Weight," Med. Eng. Phys., **35**(7), pp. 969–977.

[16] Cholewicki, J., and McGill, S. M., 1996, "Mechanical Stability of the In Vivo Lumbar Spine: Implications for Injury and Chronic Low Back Pain," Clin. Biomech., **11**(1), pp. 1–15.

[17] La Barbera, L., Brayda-Bruno, M., Liebsch, C., Villa, T., Luca, A., Galbusera, F., and Wilke, H. J., 2018, "Biomechanical Advantages of Supplemental Accessory and Satellite Rods With and Without Interbody Cages Implantation for the Stabilization of Pedicle Subtraction Osteotomy," Eur. Spine J., **27**(9), pp. 1–10.

[18] La Barbera, L., Galbusera, F., Wilke, H. J., and Villa, T., 2016, "Preclinical Evaluation of Posterior Spine Stabilization Devices: Can the Current Standards Represent Basic Everyday Life Activities?," Eur. Spine J., **25**(9), pp. 2909–2918.

[19] Sines, G., Waisman, J. L., and Dolan, T. J., 1959, *Metal Fatigue*, McGraw-Hill, New York.

[20] Rack, H. J., and Qazi, J. I., 2006, "Titanium Alloys for Biomedical Applications," Mater. Sci. Eng. C, **26**(8), pp. 1269–1277.

[21] Saitova, L. R., Höppel, H. W., Göken, M., Semenova, I. P., and Valiev, R. Z., 2009, "Cyclic Deformation Behavior and Fatigue Lives of Ultrafine-Grained Ti-6Al-4V ELI Alloy for Medical Use," Int. J. Fatigue, **31**(2), pp. 322–331.

[22] Dick, J. C., and Bourgeault, C. A., 2001, "Notch Sensitivity of Titanium Alloy, Commercially Pure Titanium, and Stainless Steel Spinal Implants," Spine, **26**(15), pp. 1668–1672.

[23] Melkerson, M. N., Griffith, S. L., and Kirkpatrick, J. S., 2003, *Spinal Implants: Are We Evaluating Them Appropriately*?, ASTM International, West Conshohocken, PA, Publication No. 1431.